JOURNAL OF Materials CHEMISTRY

Structural investigation of oxygen insertion within the $Ce_2Sn_2O_7$–$Ce_2Sn_2O_8$ pyrochlore solid solution by means of *in situ* neutron diffraction experiments

Bruno Tolla,[a] Alain Demourgues,[a,b] Olivier Isnard,[c] Michel Menetrier,[a] Michel Pouchard,*†[a] Louis Rabardel[a] and Thierry Seguelong[b]

[a]*ICMCB-CNRS, 162 avenue du Dr. A. Schweitzer, 33608 Pessac cedex, France. E-mail: pouchard@icmcb.u-bordeaux.fr*
[b]*Rhodia, Centre de Recherches d'Aubervilliers, 52 rue de la Haie Coq, F-93308 Aubervilliers cedex, France*
[c]*CNRS Cristallographie, BP 166, 38042 Grenoble cedex 9, France*

Received 22nd July 1999, Accepted 17th September 1999

The amazing oxygen exchange properties within the $Ce_2Sn_2O_7$–$Ce_2Sn_2O_8$ pyrochlore solid solution were investigated by means of *in situ* neutron diffraction experiments. The structural modification of the $Ce_2Sn_2O_7$ phase heated under oxygen up to 1000 °C was followed on the basis of the neutron diffraction patterns, continuously collected with a 5 min counting rate at 2.529 Å. The structure of the $Ce_2Sn_2O_8$ pyrochlore phase has been previously determined at room temperature on the basis of the powder neutron diffraction pattern collected at 1.594 Å. Contrary to the oxygen-intercalated zirconate pyrochlores, oxygen atoms preferentially occupy a 32e crystallographic site, which is more distant from the Sn^{4+} cation than the other interstitial 8a site. Two kinds of local oxygen defects were identified within the $Ce_2Sn_2O_{8-\varepsilon}$ ($0 \leqslant \varepsilon \leqslant 0.05$) pyrochlore at 400 °C. The most stable is a tetrahedron of oxygen atoms (32e site) around an oxygen vacancy (8b site), comparable to the Willis clusters found in UO_{2+x}. The other, lying around the 8a site, involves short oxygen–oxygen distances and constitutes a new type of oxygen cluster around tin atoms. In addition to the successive disappearance of these local defects from 400 °C to 700 °C, cerium deinsertion was detected above 500 °C. This leads to new cerium deficient $Ce_{2-x}Sn_2O_y$ phases, which exhibit structural changes. The oxygen storage capacity (OSC) of the $Ce_2Sn_2O_7$ pyrochlore was thus detailed by considering the successive insertion/deinsertion reactions and the Ce–Sn–O phase diagram.

1 Introduction

The pyrochlore structure is adopted by a large number of ternary oxides with the $A_2B_2O_7$ chemical formulation.[1] Although a lot of studies have been devoted to pyrochlores exhibiting vacancies on the A and/or O sites,[2–4] oxygen overstoichiometry had not been reported until recent works. For the first time, Thomson *et al.*[5] carried out the chemical intercalation of oxygen within the cerium(III)-based $Ce_2Zr_2O_7$ pyrochlore, and characterised an oxygen-rich pyrochlore-type phase. The $Ce(III,IV)_2Zr_2O_{7.36}$ composition was thus obtained after mild oxidation of the stoichiometric zirconate at room temperature in a 0.5 M sodium hypobromite solution. The oxygen interstitial sites were determined by the authors on the basis of neutron diffraction experiments. They remarked that the sites around the Zr^{4+} cation were the most favourable for oxygen insertion because of the chemical nature of zirconium. They furthermore characterised the oxygen sublattice reorganisation, and explained it by considering the convergence of the ionic radii of the two cations after Ce^{3+} oxidation. In the same way, EXAFS studies of the Zr K-edge of $[La(III)_{1-x}Ce(IV)_x]_2Zr_2O_{7+x}$ pyrochlores confirmed that the local coordination of Zr^{4+} shifted from 6 to 7 with oxygen insertion.[6] In addition, the CeO_2–ZrO_2 system, which had been extensively studied by Collongues *et al.*,[7] was recently reinvestigated by evolved-oxygen gas analysis (EGA) to clarify the oxygen exchange properties of several intermediate phases.[8] The authors identified a $CeZrO_4$ phase (*i.e.* $Ce_2Zr_2O_8$), with a structure close to that of the pyrochlore, but with several diffraction lines not allowed by the $Fd\bar{3}m$ space group. The oxygen mobility within this phase was remarkably enhanced compared to that in the disordered tetragonal $CeZrO_4$ phase. In a previous paper, we reported the synthesis of the new $Ce_2Sn_2O_7$ pyrochlore.[9] Thermogravimetric experiments highlighted interesting insertion/deinsertion behaviours inside this pyrochlore phase upon calcination. The new oxygen-intercalated $Ce_2Sn_2O_8$ pyrochlore phase was thus obtained at 400 °C under oxygen flow. This new compound exhibits oxygen understoichiometry from 400 to 700 °C. Furthermore, this reaction seems to be in competition with cerium oxide segregation at high temperature, leading to the formation of new cerium deficient pyrochlore phases. *In situ* neutron diffraction experiments were undertaken in order to determine the oxygen insertion sites and the insertion/deinsertion reactions involved. This paper presents the results of these structural investigations. The major differences between the reactivity of cerium(III) stannate and zirconate towards oxygen will be pointed out.

2 Experimental

The preparative methods for the $Ce_2Sn_2O_7$ and $Ce_2Sn_2O_8$ pyrochlore phases were described in a previous publication.[9] The samples were stored in sealed silica vials in order to avoid hydration and carbonation.

Thermogravimetric measurements were carried out on a TAG-24 symmetrical Setaram thermobalance which compensates for Archimedes' force. The experiments were carried out

†Institut Universitaire de France.

under oxygen flow, the heating and cooling ramps being systematically 3 °C min^{-1}. The room temperature powder neutron diffraction pattern of the $Ce_2Sn_2O_8$ phase at $\lambda = 1.594$ Å was recorded on the CRG/D2B (CNRS) beam line at the Laue–Langevin institute (ILL). Additional *in situ* experiments at 2.529 Å were performed on the D1B station. For the latter, 5 g of the $Ce_2Sn_2O_7$ sample was poured into a silica tube of 20 mm in diameter, tightly connected to a gas ramp, and evacuated for 1 h at room temperature. The sample holder was introduced inside a specially designed furnace mounted on the diffractometer. The transmitted beam was analysed by means of a multidetector covering 80°. The 2.529 Å wavelength, selected by the (002) reflection of a pyrolytic graphite monochromator, provides a high neutronic flux (6.5×10^6 n cm^{-2} s^{-1}), in such a way that the diffraction patterns could be continuously collected in 5 min with sufficient statistics.

The ^{119}Sn NMR spectra of $Ce_2Sn_2O_8$ were recorded on a Bruker MSL 200 spectrometer (4.7 T magnet) operating at 74.5 MHz. MAS spectra were undertaken at various spinning speeds up to 15 KHz, by means of a single pulse sequence with phase cycling. Relaxation times were estimated with a saturation sequence. SnO_2 was used as a secondary reference for the ppm scale (−604.3 ppm with respect to Me_4Sn).

3 Results and discussion

The oxygen exchange properties of the $Ce_2Sn_2O_7$ phase were characterised by thermogravimetric experiments under O_2 (Fig. 1), as previously described.[9]

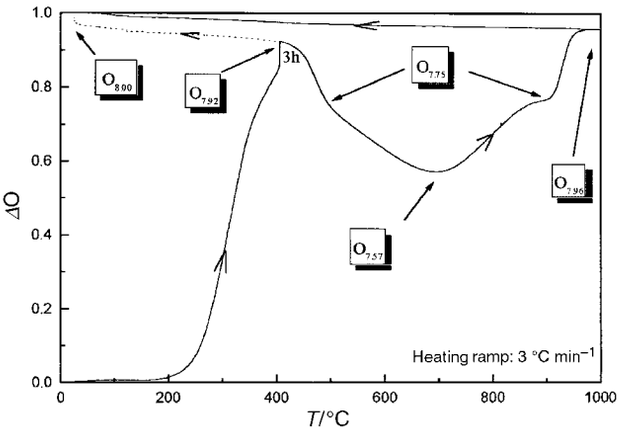

Fig. 1 Thermogram of $Ce_2Sn_2O_7$ under oxygen flow.[9] Solid line: oxidation up to 1000 °C, with an intermediate 3 h stage at 400 °C, and cooling to room temperature. Dotted line: cooling to room temperature after the intermediate stage.

3.1 Structural characterisation of the $Ce_2Sn_2O_8$ pyrochlore

3.1.1 Rietveld-type structural refinements. Room temperature X-ray and electron diffraction experiments led us to assign the pyrochlore structure to the $Ce_2Sn_2O_8$ phase.[9] Rietveld-type structural refinements were carried out on the basis of the room temperature neutron diffraction pattern collected at $\lambda = 1.594$ Å. This presents 73 independent reflection lines among which 51 are exploitable according to their resolution. Rietveld-type structural refinements were performed by means of the FullProf program.[10] The background function results from the linear interpolation of 26 arbitrarily selected points. The origin shift is calculated from the unit cell parameter of $Ce_2Sn_2O_8$, which was previously refined on its X-ray diffraction pattern. The intensities were calculated by means of a pseudo-Voigt function, the width of the reflection lines varying according to the function determined by Caglioti *et al.*[11] The structural variables were refined simultaneously, except the oxygen thermal parameters which were set to unity. These were refined afterwards, the occupancy factors and positional parameters then being fixed, because of their strong correlation with the other variables. Under these conditions, the number of refined parameters, $N = 16$ is rather small in comparison with the number of independent reflections. We first verified that the cerium and tin cations remained on their regular 16d (1/2,1/2,1/2) and 16c (0,0,0) sites, respectively, no cationic site disorder being observed. It should be pointed out that the origin is not the same as that chosen by Thomson.[5] The $Ce_2Sn_2O_7$ pyrochlore structure was then used as a starting model for the refinement. The various insertion sites within the pyrochlore network (8a, 32e) and the possible rearrangement of the oxygen subarray were then tested. Table 1 groups the different structural models considered during the refinement, together with the associated number of refined parameters (N) and the corresponding Rietveld reliability factors. The final atomic coordinates, site occupancies, thermal parameters and interatomic distances are detailed in Table 2. The observed, calculated and difference profiles are plotted in Fig. 2.

The 32e ($x = 1/4$) crystallographic site corresponds to the cationic vacancies eight-fold coordinated to oxygen in the parent fluorite structure (space group $Fm\bar{3}m$). The 8a (1/8,1/8,1/8) site is related to the vacancies created on the oxygen subarray of fluorite to obtain the pyrochlore structure. In contrast to the $Ce_2Zr_2O_{7.36}$ pyrochlore,[5] a 32e interstitial site seems to be the most favourable for oxygen insertion: 25% of the 32e (0.290,0.290,0.290) crystallographic sites are found to be occupied by oxygen atoms. This corresponds to one oxygen per formula unit, leading to the formal composition $Ce_2Sn_2O_8$ [Table 1, row (3)]. However, the refined oxygen occupancy in the 8b site shifts from 1 to 0.75 [Table 1, row (4)]. Indeed, it can be remarked that an 8b (3/8,3/8,3/8) site is surrounded by a tetrahedron of 32e sites, which were displaced from the normal site (1/4,1/4,1/4) towards the 8b site. As the distance between 8b and 32e sites is very short ($d = 1.55$ Å), it can therefore be inferred that the oxygen atoms inserted in 25% of the 32e sites form regular tetrahedra around the 8b sites, which are unoccupied. This oxygen cluster model is in good agreement with the refined occupancy of the 8b site, as the insertion of 1 oxygen per formula unit in 32e sites results in the occurrence of vacancies in 25% of the 8b sites. This kind of local defect has already been observed by Willis in the UO_{2+x} overstoichiometric fluorite phases.[12] In contrast to Zr^{4+}, which is preferentially seven-coordinate in oxides such as monoclinic zirconia, Sn^{4+} is only known in octahedral coordination. This explains why oxygen is more likely to be inserted in the 32e site of the stannate pyrochlore, rather than in the 8a site which is at

Table 1 Structural refinement of the $Ce_2Sn_2O_8$ phase based on its room-temperature neutron diffraction pattern: evolution of the Rietveld reliability factors with the different structural models considered to describe oxygen insertion

Chemical formulation	R_p (%)	R_{wp} (%)	χ^2	R_B (%)	N
(1) $Ce_2{}^{16d}Sn_2{}^{16c}O_6{}^{48f(i)}O_1{}^{8b}$	28.5	27.7	8.74	20.34	8
(2) $Ce_2{}^{16d}Sn_2{}^{16c}O_6{}^{48f(i)}O_1{}^{8b}O_1{}^{8a}$	38.4	39.6	17.8	30.32	8
(3) $Ce_2{}^{16d}Sn_2{}^{16c}O_6{}^{48f(i)}O_1{}^{8b}O_1{}^{32e}$	21.2	19.0	4.09	12.89	9
(4) $Ce_2{}^{16d}Sn_2{}^{16c}O_6{}^{48f(i)}O_{0.75}{}^{8b}O_{1.00}{}^{32e}$	19.4	17.0	3.30	10.92	11
(5) $Ce_2{}^{16d}Sn_2{}^{16c}O_{4.76}{}^{48f(i)}O_{0.15}{}^{48f(ii)}O_{1.26}{}^{48f(iii)}O_{0.75}{}^{8b}O_{1.05}{}^{32e}$	13.6	12.1	1.66	4.79	16

Table 2 Final refinement: structural and thermal parameters for $Ce_2Sn_2O_8$

Atom	Site	*x/a*	*y/a*	*z/a*	B_{iso}/Å^2	Occupancy *N*	
Ce	16d	1/2	1/2	1/2	1.03(8)	2	
Sn	16c	0	0	0	0.30(5)	2	
O1	8b	3/8	3/8	3/8	0.67(14)	0.75(2)	
O2	32e	0.2864(5)	0.2864(5)	0.2864(5)	0.34(14)	1.05(2)	
O3	48f(i)	0.3302(5)	1/8	1/8	1.05(3)	4.76(9)	
O4	48f(ii)	0.1506(91)	1/8	1/8	2.00(69)	0.15(2)	
O5	48f(iii)	0.3706(19)	1/8	1/8	0.97(14)	1.26(7)	
	R_p (%) 13.6	R_{wp} (%) 12.1	R_{exp} (%) 9.36	χ^2 1.66	R_B (%) 4.79	ΣOcc. = 7.97	
Bond	Ce–O1	Ce–O2	Ce–O5	Sn–O3	Sn–O4	Sn–O5	O4–O5
d/Å	2.284	2.317(2)	2.311(5)	2.048(2)	2.139(29)	2.258(6)	2.321(48)

the center of a Sn^{4+} tetrahedron. Furthermore, the coordination of Ce shifts from (2+6) to (4+6) around this local defect, as one 8b coordinating oxygen is replaced by three 32e atoms on the side of the tetrahedron (Fig. 3). This description concerns 50% of the cerium atoms, the other half remaining in their initial (2+6) coordination mode.

At this stage of our refinement, the chemical formulation is $Ce_2Sn_2O_{7.75}$, which is inconsistent with the results of the thermogravimetric analysis. Actually, the refinement reveals the presence of a small atomic density around the 8a sites, associated with the displacement of part of the normal oxygen atoms in 48f (x_1,1/8,1/8) sites towards a less relaxed position (x_3,1/8,1/8), $x_3 > x_1$ [Table 1, row (5)]. Indeed, the 8a position is surrounded by an octahedron of O^{2-} ions (48f sites), and a tetrahedron of Sn^{4+} ions (16c sites). Introducing an oxygen atom around the 8a site will therefore imply the relaxation of the surrounding ones in 48f sites due to the electrostatic repulsion (Fig. 4). The best fit between experimental and calculated data was obtained by placing the interstitial oxygen between the 8a (1/8,1/8,1/8) and 48f (x_3,1/8,1/8) sites, *i.e.* in another 48f site (x_2,1/8,1/8) with $1/8 < x_2 < x_3$. We also verified that when the interstitial atom was fixed into the 8a site, its occupancy parameter returned to zero. Three kinds of oxygen atoms in 48f sites are then obtained within the $Ce_2Sn_2O_8$ structure (Table 2): (i) those in the normal 48f site (0.3302(5),1/8,1/8) which is close to the original one (0.3311(2),1/8,1/8) within the $Ce_2Sn_2O_7$ pyrochlore, (ii) the oxygen inserted near the 8a site (0.1506(91),1/8,1/8), and (iii) the nearest (i) oxygen atom which relaxed from its normal position [$x = 0.3302(5)$] to a more distant one [$x = 0.3706(19)$]. As the latter 48f(iii) oxygen position is displaced towards cerium, it enters the first coordination sphere of cerium (Table 2). The coordination of cerium thus shifts from (2+6) to (3+5) around this local defect, or (4+4) if two defects are close together.

Fig. 5 describes the new coordination polyhedron of tin, whose local coordination becomes [3(2.05 Å)+1(2.14 Å)+3(2.26 Å)] around this defect. The short O4–O5 distance ($d = 2.32$ Å) involved by the insertion of O4 is outlined. The shift of the local coordination of tin from six to seven can be explained, from a steric point of view, by this short distance which could account for a slight interaction between the oxygen atoms involved. The same explanation was given for the unusual coordination numbers of some peroxo complexes, such as $[Mo(O_2)_4]^{2-}$,[13] where the O–O distances are much smaller (*ca.* 1.5 Å). The refined occupancies of the 48f sites agree with our structural model, as the *N*[48f(ii)] : *N*[48f(iii)] ratio (Table 2) is substantially lower than 1 : 1 (1 : 6 theoretically). This implies that the occurrence of the interstitial O4 oxygen atom affects the six O5 atoms which are displaced from their normal O3 positions. It can also be inferred that the former are delocalised on the 6 equivalent 48f(ii) sites present within this octahedron. However, taking into account the low accuracy of the 48f(iii) occupation number (Table 2), it is difficult to go into further detail. According to the low x_2 value, close to 1/8, it can be asserted that a single atom is inserted within an O5 octahedron, whether delocalised or not. As the latter is situated in an Sn^{4+} tetrahedron as mentioned earlier, this defect concerns about 30% of the tin atoms. It has to be pointed out that the O4 positional parameter is less accurate than the others, and that its Debye–Waller factor is unusually high. The delocalisation of O4 atoms, inducing the dynamic relaxation of the others in 48f sites, could be the origin of these features. Willis[12] has encountered the same phenomenon with one of the interstitial oxygen atoms in the UO_{2+x} fluorite-type oxide.

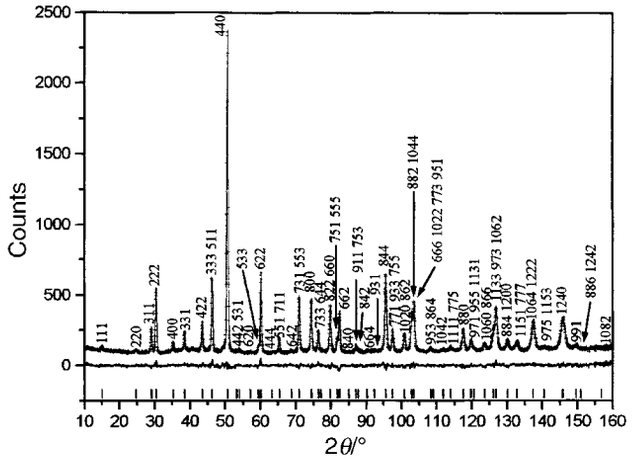

Fig. 2 Experimental (crosses) and calculated (solid line) neutron diffraction profiles for the $Ce_2Sn_2O_8$ pyrochlore. The lower line is the difference function.

3.1.2 ^{119}Sn MAS-NMR spectroscopy. We have shown that an appreciable amount of interstitial oxygen atoms lie around the 8a site of the $Ce_2Sn_2O_8$ phase. According to our model, the

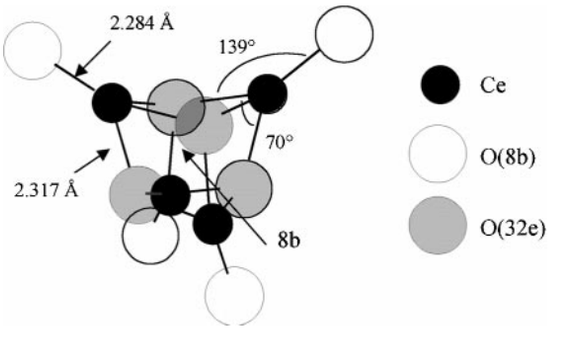

Fig. 3 Local environment of cerium around the 32e oxygen defect, within the $Ce_2Sn_2O_8$ pyrochlore.

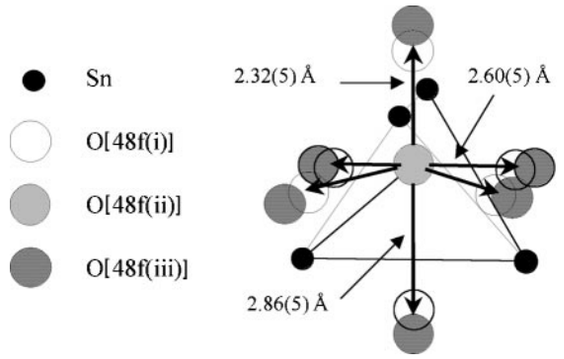

Fig. 4 Local environment around the 48f(ii)/8a oxygen defect within the $Ce_2Sn_2O_8$ pyrochlore. The arrows show the influence of the inserted 48f(ii) atom on 48f(i) and 48f(iii), according to our structural investigations.

30% of the Sn^{4+} cations which surround this defect are unusually [3(2.05 Å)+1(2.14 Å)+3(2.26 Å)] coordinated. ^{119}Sn NMR spectroscopy was thus carried out in order to confirm such a local environment of tin in the pyrochlore network.

The static NMR spectrum of the $Ce_2Sn_2O_8$ phase presents two relatively narrow resonance bands; at 15 KHz they are reduced to the two corresponding isotropic bands, with no spinning sidebands (Fig. 6). The chemical shift of the most intense band (−670 ppm with respect to Me_4Sn) is close to those reported for the single bands of the diamagnetic stannates, *i.e.* $La_2Sn_2O_7$ (−642 ppm), $Lu_2Sn_2O_7$ (−562 ppm) and $Y_2Sn_2O_7$ (−582 ppm).[14] This band thus corresponds to Sn^{4+} cations which are in distorted octahedral coordination spheres (D_{3d}), identical to those found in stoichiometric $Ln_2Sn_2O_7$ pyrochlores. The other band (−872 ppm with respect to Me_4Sn), which is shifted out of the diamagnetic stannates domain, reveals the presence of a different environment for part of the Sn^{4+} cations within the $Ce_2Sn_2O_8$ pyrochlore. Its chemical shift with respect to the first band (−202 ppm) implies either an interaction with an unpaired electron (Fermi contact), or a modification in the Sn^{4+} environment. However, the spin–lattice relaxation times of the two bands are close (*ca.* 1 s), therefore the first possibility is ruled out. Furthermore, the ^{119}Sn NMR studies of organostannic compounds provide a set of remarkable data for tetravalent tin in various coordination modes. Indeed, it appears from the MAS-NMR studies of Reuter *et al.*[15] and Kümmerlen *et al.*[16] that the addition of one oxygen atom to the coordination sphere of tin results in a change in the chemical shift by −150 to −250 ppm. Thus, assuming that the ionicity difference in Sn–O bindings from organostannic phases to oxides introduces an overall displacement of the chemical shifts but doesn't modify their evolution with the Sn^{4+} coordination number, it can be concluded that the resonance line situated at −872 ppm with respect to Me_4Sn characterises a seven-coordinate Sn^{4+} cation. On the other hand, the integration of the bands proves that the latter concerns exactly 30% of the tin atoms within the $Ce_2Sn_2O_8$ pyrochlore (Fig. 6). Those

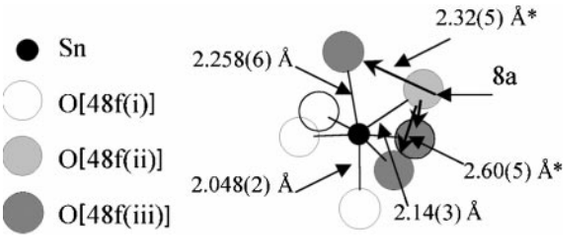

Fig. 5 Modification of the local environment of tin (30%) around the 48f(ii)/8a defect. The shortest O–O distances are outlined (*).

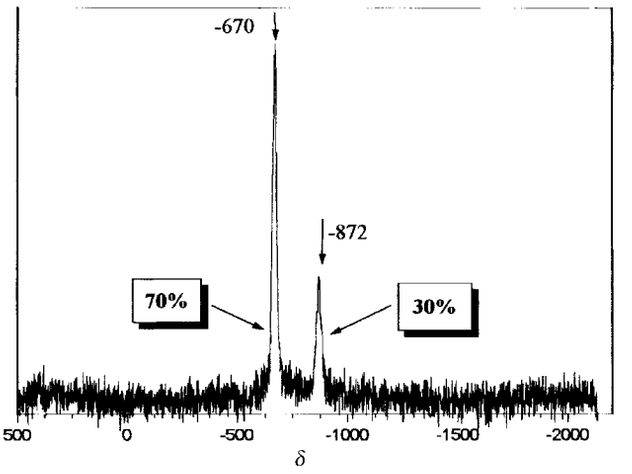

Fig. 6 ^{119}Sn MAS-NMR spectrum of $Ce_2Sn_2O_8$ (single pulse sequence; spinning speed: 15 KHz; referenced to Me_4Sn).

spectroscopic results are thus in perfect agreement with the structural refinements based on neutron data.

3.2 Investigation of oxygen exchange phenomena in the $Ce_2Sn_2O_7$–$Ce_2Sn_2O_8$ pyrochlore solid solution

The structural evolution of the $Ce_2Sn_2O_7$–$Ce_2Sn_2O_8$ pyrochlore solid solution *versus* oxygen stoichiometry was continuously followed from 25 to 1000 °C. An initial diffraction pattern of $Ce_2Sn_2O_7$ was recorded under vacuum at room temperature for reference. Standard oxygen was then introduced into the circuit, its partial pressure being fixed at 1 atm, and the sample was subsequently heated. The temperature profile adopted for these *in situ* neutron diffraction experiments was the same as that employed for the thermogravimetric analysis presented in Fig. 1. However, the stage at 400 °C was longer in the former experiments (5 h), because it involved larger amounts of products. We nevertheless observed that the diffraction patterns collected every 5 min did not change after 3 h. The crystal structure analysis was undertaken with the same procedure as for the refinement of the room temperature neutron diffraction pattern. However, it should be pointed out that, given the $\lambda = 2.529$ Å wavelength used, the number of experimental points and exploitable peaks is greatly reduced ($N = 12$). We therefore limited the refined variables to the structural and thermal ones, all the others being determined and fixed at room temperature by considering the parameters of the $Ce_2Sn_2O_7$ reference diffraction pattern.

An initial Rietveld-type refinement was carried out by considering the neutron diffraction patterns accumulated in the last 50 min of the heating stage at 400 °C. Despite its lower accuracy, this refinement leads to the same results as those obtained from the room temperature neutron diffraction pattern of $Ce_2Sn_2O_8$. It should be noted that the slight oxygen shift from room temperature ($Ce_2Sn_2O_8$) to 400 °C ($Ce_2Sn_2O_{7.91}$) detected by thermogravimetric analysis (Fig. 1) cannot be confirmed by these refinements, given the uncertainties in the crystallographic site occupancies.

The structural modification of the $Ce_2Sn_2O_7$–$Ce_2Sn_2O_8$ pyrochlore solid solution *versus* oxygen stoichiometry was then continuously followed from 400 to 1000 °C. Because of the low statistics, the thermal parameters were fixed to the values refined at 400 °C, which already presented low accuracy. Rather than the structural parameters (unit cell parameter and site occupancies) absolute values, whose uncertainty increases with temperature, it is their evolution along the thermal cycle which provides useful information (Fig. 7, 8).

We have already characterised the reversible oxygen deinsertion from the $Ce_2Sn_2O_8$ pyrochlore in the 400–500 °C domain. Thermogravimetric experiments highlighted the

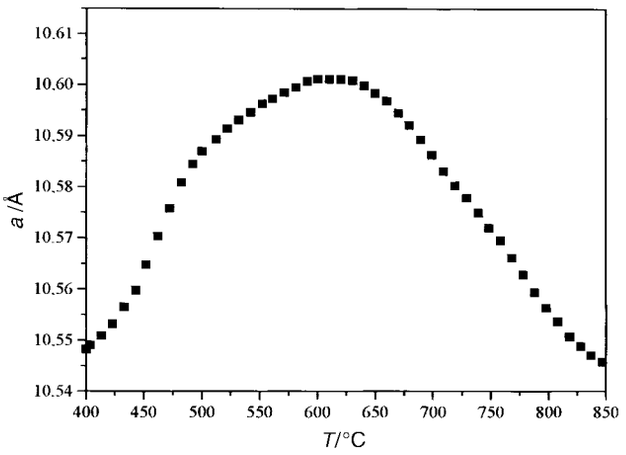

Fig. 7 Evolution of the unit cell parameter of the cerium stannate pyrochlore under O_2 from 400 to 850 °C.

bivariant redox equilibrium associated with reaction (1):

$$Ce(IV)_2Sn_2O_8 \rightleftharpoons Ce(III,IV)_2Sn_2O_{8-\delta} + \delta/2O_2 \quad (0 < \delta < 0.25) \qquad (1)$$

The partial reduction of Ce^{4+} to Ce^{3+} is characterised by the increase of the unit cell parameter above 400 °C (Fig. 7). The oxygen atoms inserted near the 8a site are mainly involved in this reaction, as the occupancy numbers of the 48f(ii) and 48f(iii) oxygen atoms tend to zero, while that of 48f(i) returns to 6 (Fig. 8). Oxygen clusters in 32e sites are thus the only local defect within the $Ce_2Sn_2O_{7.75}$ pyrochlore obtained around 500 °C.

The $Ce_2Sn_2O_8$ pyrochlores heated for several hours near 700 °C present a colour change from yellow to green. We remarked that the X-ray diffraction patterns of the samples recovered at room temperature indicated a structural modification of the pyrochlore, associated with the appearance of CeO_2 as an impurity phase.[9] Thus, additional reflection lines, which are incompatible with the *F* Bravais mode of the $Fd\bar{3}m$ space group, but allowed in a primitive cubic unit cell, were detected at low angles. Furthermore, the unit cell parameter of the product recovered at room temperature decreases compared to that of $Ce_2Sn_2O_8$. Fig. 8 indicates that a cerium deinsertion reaction actually interferes with reaction (1). Indeed, the 16d site occupancy notably decreases above 600 °C (Fig. 8), and it is formalised by reaction (1′):

$$Ce_2(III,IV)Sn_2O_{8-\delta} \rightarrow Ce_{2-x}(III,IV)Sn_2O_{8-\delta-2x} + xCeO_2 \quad (x < (1-\delta)/2) \qquad (1')$$

However, this reaction involves a partial reduction of Ce^{4+} within the pyrochlore phase, so that equilibrium (1) should be displaced toward the oxidation of cerium. Thus, a combination of reaction (1′) and the reverse of (1) leads to reaction (2):

$$Ce_2(III,IV)Sn_2O_{8-\delta} + xO_2 \rightarrow Ce_{2-x}(III,IV)Sn_2O_{8-\delta} + xCeO_2 \quad (x < \delta/2) \qquad (2)$$

As reaction (2) implies a mass gain, it explains the slope change of the TGA curve around 500 °C. It also involves Ce^{3+} oxidation, so that the higher extent of cerium deinsertion is reached when $x = \delta/2$, as all the cerium is tetravalent. It can therefore be concluded that the pyrochlore with the largest amount of vacancies which can be obtained through reaction (2) has the $Ce_{1.5}^{4+}Sn_2^{4+}O_7$ chemical formulation, assuming $\delta \leqslant 1$. The contraction of the structure due to Ce^{3+} oxidation and its deinsertion is detected above 630 °C, as reaction (2) becomes predominant over reaction (1).

Reaction (2) is irreversible and kinetically governed, in contrast to the reversible reaction (1), which is governed by thermodynamics. Thus, the oxygen loss is not reversible when reaction (2) interferes, as a noticeable mass gain appears during the heating stage, its extent depending upon time and temperature. Furthermore, the oxygen stoichiometry does not return exactly to O_8 as the temperature decreases, which demonstrates that the oxidation reaction (3) does not go to completion.

$$Ce(III,IV)_{2-x}Sn_2O_{8-\delta} + (\delta-2x)/2O_2 \rightleftharpoons Ce_{2-x}(IV)Sn_2O_{8-2x} \quad (x < \delta/2) \qquad (3)$$

The A-site lacunar pyrochlore recovered at room temperature therefore presents a Ce^{4+}/Ce^{3+} mixed valence. This was confirmed by means of magnetic measurements and UV-VIS diffuse reflectance spectroscopy which revealed that the as-prepared samples were paramagnetic and presented an intervalence band which accounts for their colour change. It should be noted that, in contrast to the room temperature X-ray diffraction experiments, the additional diffraction lines are not detected along the heating ramp by *in situ* neutron diffraction experiments. The reorganisation of the lattice would thus occur upon cooling, as the sample is reoxidised.

The chemical formulation of the pyrochlore obtained from reaction (1) and (2) at 700 °C is close to $Ce_{1.75}Sn_2O_7$, according to Table 3. The composition of the mixture ($Ce_{1.75}Sn_2O_7 + 0.25CeO_2$) then agrees with the oxygen stoichiometry given by the thermogravimetric analysis (Fig. 1). The remaining 8b and 48f oxygen sites corresponding to the normal sites of the stoichiometric pyrochlore should be more stable. However, we can not exclude a few oxygen 8b vacancies induced by the cerium ones. The evolution of the product is therefore driven by a type (2) reaction, with $\delta = 1$:

$$Ce_{1.75}(III,IV)Sn_2O_7 + xO_2 \rightarrow Ce_{1.75-x}(III,IV)Sn_2O_7 + xCeO_2 \quad (x < 1/4) \qquad (2')$$

This reaction is characterised by the first mass gain observed from 700 to 900 °C (Fig. 1). The $O_{7.75}$ oxygen stoichiometry at 900 °C corresponds to the ($Ce_{1.625}Sn_2O_7 + 0.375CeO_2$) mixture. The neutron diffraction experiments gave the $Ce_{1.55}Sn_2O_7$ chemical formulation at 900 °C (Fig. 8), but with a low accuracy. This is due to the large quantity of the CeO_2 segregated phase and the high value of the Debye–Waller factors, which lead to a widening of the diffraction lines intensity. The $Ce_{1.5}Sn_2O_7$ theoretical composition which can be obtained through reaction (2) should be reached by a heating stage in this domain.

The decomposition of the A-site lacunar pyrochlore was detected above 900 °C by *in situ* neutron diffraction experiments, and is related to the last mass gain on the thermogram (Fig. 1) according to reaction (4)

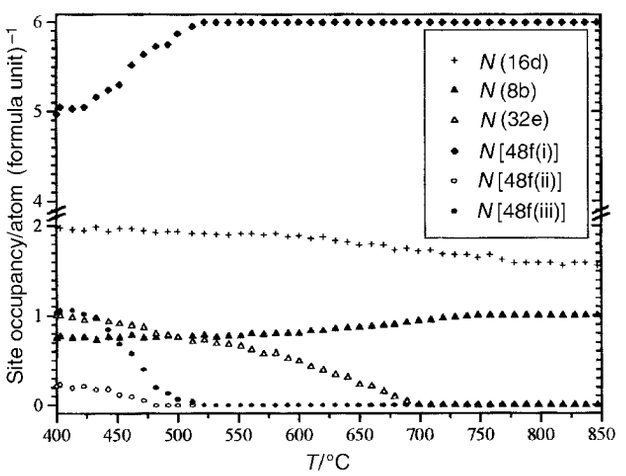

Fig. 8 Evolution of the crystallographic site occupancies within the cerium stannate pyrochlore under O_2 from 400 to 850 °C.

Table 3 Crystallographic site occupancies and unit cell parameters of the cerium stannate pyrochlore under oxygen at selected temperatures, calculated from powder neutron diffraction data

	452 °C	502 °C	551 °C	600 °C	650 °C	699 °C
a/Å	10.5648(5)	10.5870(6)	10.5963(6)	10.6011(8)	10.5984(10)	10.5863(16)
Occupancy						
Ce(16d)	1.97(2)	1.94(3)	1.92(3)	1.89(5)	1.79(6)	1.72(9)
Sn(16c)	2	2	2	2	2	2
O(8b)	0.75(1)	0.76(2)	0.77(2)	0.79(3)	0.87(4)	0.94(6)
O(32e)	0.91(2)	0.76(2)	0.66(3)	0.50(5)	0.23(7)	0.01(11)
O[48f(i)]	5.30(5)	5.87(6)	6	6	6	6
O[48f(ii)]	0.11(2)	0	0	0	0	0
O[48f(iii)]	0.68(4)	0.06(5)	0	0	0	0
Reliability factors						
R_p (%)	13.7	15.9	15.7	17.4	19.3	25.6
R_{wp} (%)	9.27	10.9	12.7	12.1	14.0	19.1
R_{exp} (%)	5.92	5.92	5.96	6.09	6.19	6.26
R_B (%)	5.34	4.66	5.57	5.93	7.87	13.5

$$Ce_{1.625}Sn_2O_7 + 0.125O_2 \rightarrow 1.625CeO_2 + 2SnO_2 \quad (4)$$

As for reaction (2), it should be noted that given its kinetic nature, this decomposition should start at a temperature lower than 900 °C, although this was not detected by *in situ* measurements.

4 Conclusion

The $Ce_2Sn_2O_7$–$Ce_2Sn_2O_8$ pyrochlore solid solution exhibits high oxygen exchange at low temperature, as was already observed in the homologous cerium zirconate system. The amazing oxygen exchange properties of the $Ce_2Sn_2O_7$ pyrochlore, characterised by thermogravimetric experiments, were related to the structural evolution of the phase. Room temperature neutron diffraction experiments allowed us to determine the oxygen insertion sites within the $Ce_2Sn_2O_8$ pyrochlore. It appeared that two kinds of oxygen defects were created inside the pyrochlore matrix upon oxygen insertion. The major one is a tetrahedron of oxygen atoms in 32e sites associated with an 8b vacancy, comparable to the Willis clusters found in UO_{2+x}. The other is situated close to 8a sites and implies that the local coordination of part of the Sn^{4+} cations (30%) shifts from six to seven. This unexpected result was confirmed by a ^{119}Sn MAS-NMR study of the $Ce_2Sn_2O_8$ phase. *In situ* neutron diffraction experiments were then carried out in order to follow the evolution of the previously characterised oxygen defects along the thermal cycle. The Rietveld-type structural refinements outlined two successive deinsertion reactions. An initial reversible oxygen deinsertion, which is thermodynamically driven, occurs above 400 °C: it appears that the oxygen cluster in the 32e site remains the most stable interstitial species with respect to temperature. This is followed by a second irreversible kinetic ceria phase separation above 500 °C, which explains why the $Ce_2Sn_2O_{8-\delta}$ pyrochlore is only stable through thermal cycling up to this temperature. All of the reactions involved along the thermal cycle were replaced within the ternary diagram given in Fig. 9. It can be emphasised that the compositional domain of the lacunar pyrochlore above 400 °C lies within the (A,C,D,F) quadrilateral, the chemical formulation depending on the heating rate.

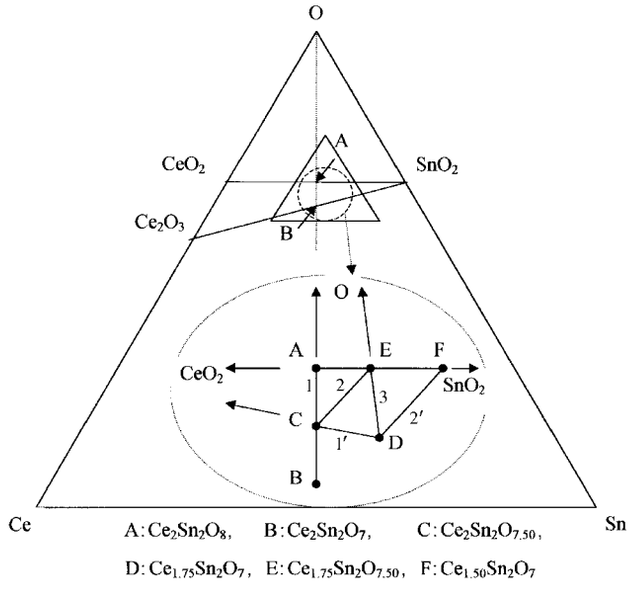

Fig. 9 Detail of the schematic Ce–Sn–O ternary diagram.

Acknowledgements

This work has been supported by the Rhodia Society. We are particularly indebted to D. Denux, C. Sourisseau and J.-C. Grenier for their valuable assistance.

References

1 M. A. Subramanian, G. Aravamudan and G. V. S. Rao, *Prog. Solid State Chem.*, 1983, **15**, 55.
2 A. W. Sleight, *Mater. Res. Bull.*, 1969, **4**, 377.
3 C. Michel, D. Groult and B. Raveau, *Mater. Res. Bull.*, 1973, **8**, 201; 451; *J. Inorg. Nucl. Chem.*, 1975, **37**, 247.
4 B. Darriet, M. Rat, J. Galy and P. Hagenmuller, *Mater. Res. Bull.*, 1971, **6**, 1305.
5 J. B. Thomson, A. R. Armstrong and P. G. Bruce, *J. Am. Chem. Soc.*, 1996, **118**, 11 129.
6 H. Yokoi, Y. Arita, T. Matsui, H. Ohno and K. Kobayashi, *J. Nucl. Mater.*, 1996, **238**, 163.
7 R. Collongues, M. Perez, Y. Jorba and J. Lefèvre, *Bull. Soc. Chim. Fr.*, 1961, **70**, 70.
8 S. Otsuka-Yao-Matsuo, N. Izu, T. Omata and K. Ikeda, *J. Electrochem. Soc.*, 1998, **145**, 1406; S. Otsuka-Yao-Matsuo, T. Omata, N. Izu and H. Kishimoto, *J. Solid State Chem.*, 1998, **138**, 47.
9 B. Tolla, A. Demourgues, M. Pouchard, L. Rabardel, L. Fournès and A. Wattiaux, *C. R. Acad. Sci. (Paris), Sér. IIc*, 1999, **2**, 139.
10 J. Rodriguez-Caravajal, in *Collected Abstracts of the Powder Diffraction Meeting*, Toulouse, France, 1990, p. 127.
11 G. Caglioti, A. Paoletti and F. P. Ricci, *Nucl. Instrum. Methods*, 1958, **3**, 223.
12 B. T. M. Willis, *J. Phys. (Paris)*, 1964, **25**, 431.
13 A. F. Wells, *Structural Inorganic Chemistry*, Oxford Science Publication, 1984.
14 C. P. Grey, C. M. Dobson, A. K. Cheetham and R. J. B. Jakeman, *J. Am. Chem. Soc.*, 1989, **111**, 505.
15 H. Reuter and A. Sebald, *Z. Naturforsch., Teil B*, 1993, **48**, 195.
16 J. Kümmerlen, A. Sebald and H. Reuter, *J. Organometal. Chem.*, 1992, **427**, 309.

Paper 9/05914H